2019 DIE CASTING CONGRESS &TABLETOP
NADCA
NORTH AMERICAN DIE CASTING ASSOCIATION



# Effect of Zinc Alloy Casting Section Thickness on Creep Behavior

T. Frank, A. Kansy, L. Kallien, W. Leis

GTA Foundry Technology Aalen,

F.E. Goodwin

International Zinc Association

## ABSTRACT

Zinc die casting alloys are susceptible to creep because of their low melting temperature. In this study we investigated the creep behavior of zinc alloy 5 under uniaxial tensile load. Before starting the creep tests, the specimens were artificially aged by a heat treatment at 95 °C for 7 days to avoid subsequent natural ageing and to achieve a targeted microstructure. The applied temperatures for the creep tests were 60 °C, 90 °C and 120 °C, the applied loads were 10 MPa, 30 MPa and 60 MPa (1450, 4350 and 8700 psi) and the specimen thicknesses were 0.8 mm, 1.5 mm and 3.0 mm. Creep strain as a function of time was recorded in time intervals between 3 minutes and 1 hour, depending on the creep rate. Stress exponents of 3.0 – 8.6 and activation energies between 84-156 kJ/mol were determined at the applied testing conditions. Casting microstructure was found to strongly influence creep rate; observations relating microstructural features to creep rate will be described.

## INTRODUCTION

Zinc alloy 5 is the most common zinc die casting alloy and is used for structural and decorative parts for automotive, architectural, furniture, electrical and electronic applications. The alloy can be cast cost-effectively and with high productivity into near-net-shape components using the hot chamber die casting process [1]. Due to their low solidus temperatures, most zinc die casting alloys including alloy 5 tend to gradually deform plastically even at room temperature and low stresses [2]. Knowledge of the behavior of stress and temperature-related creep processes is of great importance for the design of mechanically stressed components. The aim of this study is to investigate the influence of the thickness of die cast zinc samples on creep behavior and to investigate underlying mechanisms and microstructural influences.

## DESIGN OF EXPERIMENTS

### EXPERIMENTAL METHODS

Samples with wall thicknesses of 0.8 mm, 1.5 mm and 3 mm were cast on the hot chamber die casting machine Frech DAW 80. The chemical compositions of the samples were determined via atomic emission spectrometry and is listed in Table 1. The 3.0 mm sample has a slightly different aluminum content due to the use of a different alloy batch. A die temperature of 200 °C and a gate of 55 m/s were set as casting parameters. After casting, the sample width was reduced to 14 mm and the ejection points removed by milling, so that the final dimensions were 130 mm x 14 mm x 0.8/1.5/3.0 mm. The samples were then artificially aged at 95 °C for 7 days and stored at -24 °C to prevent further ageing processes until the test procedure was begun.

To prepare for the creep tests, two clamping devices, upper and lower, were attached to the side of the specimen. The area between the clamping devices corresponds to the creep length to be investigated and is 88 mm. The specimen was attached to the creep testing machine via the upper and lower clamping devices and fitted with a thermocouple. A hollow cylindrical

furnace was placed over the specimen and raised to the test temperature. As soon as the desired temperature at the sample was reached, the desired load was applied through the lower clamping device and the recording of the measured values begin in time intervals between 3 minutes and 1 hour, depending on the creep rate.

For microstructural analysis, the samples were cut, embedded in epoxy resin and cured. Then they were ground using grit of increasing fineness, up to 2000, and then and polished using diamond suspensions with particle diameters of 2 µm and 0.05 µm. The polished samples were then etched in 0.5%-Nital solution containing 0.5 % nitric acid and 99.5 % ethanol. The etching time was 15 seconds.

***Table 1-Chemical composition of the investigated samples***

| Alloy 5 | Mg | Cu | Al | Zn |
|---|---|---|---|---|
| Standard values | 0.025 – 0.05 % | 0.7 – 1.2 % | 3.7 – 4.3 % | Balance |
| 0.8 mm | 0.031 % | 0.953 % | 3,747 % | Balance |
| 1.5 mm | 0.036 % | 0.939 % | 3,861 % | Balance |
| 3.0 mm | 0.037 % | 0.969 % | 4,212 % | Balance |

## CREEP EQUATIONS

Creep rates are calculated using slopes obtained of the creep curves (elongation over time). For the results described here, the curves describing primary creep, up to an elongation of 1%, are approximated by the function $\varepsilon = c \bullet t^a$ and the parameters a and c are determined. From this, the creep time is calculated until 1 % strain is reached:

$$t = \left(\frac{\varepsilon}{c}\right)^{\frac{1}{a}} \quad (1)$$

Where

t = creep time [s]
ε = elongation

The creep rate $\dot{\varepsilon}$ can be calculated by differentiating the creep strain with respect to time and using the creep time until 1 % strain is reached:

$$\dot{\varepsilon} = \frac{d\varepsilon}{dt} = a \cdot c \cdot t^{a-1} \quad (2)$$

### Calculation of activation energies

The creep rate can be expressed by the temperature-dependent version of Norton's law:

$$\dot{\varepsilon} = A \cdot \left(\frac{\sigma}{G}\right)^n \cdot e^{-\frac{Q}{RT}} \quad (3)$$

where

$\dot{\varepsilon}$ = creep rate [1/s]
A = creep coefficient [1/s]
σ = stress [MPa]
G = shear modulus [MPa]
n = stress exponent
Q = activation energy [J/mol]
R = gas constant [8.314 J/mol•K]
T = temperature [K]

By taking the logarithm of Equation 3 and plotting ln $\dot{\varepsilon}$ against 1/T, the activation energy Q can be determined by the slope of the straight line:

$$\ln \dot{\varepsilon} = \ln A + n \cdot \ln\left(\frac{\sigma}{G}\right) - \frac{Q}{R}\frac{1}{T} \quad (4)$$

### Calculation of stress exponent n

The stress exponent can be determined by plotting the creep rate $\dot{\varepsilon}$ against the stress σ on a log-log graph. The slope of the plotted curve corresponds to the stress exponent.

Calculation of creep constant A

The creep constant A can be determined by rearranging equation (3):

$$A = \dot{\varepsilon} \cdot \left(\frac{G}{\sigma}\right)^n \cdot e^{+\frac{Q}{RT}} \qquad (5)$$

## RESULTS

### CREEP EXPERIMENTS

The creep curves obtained at temperatures of 60, 90 and 120 °C, stresses of 10, 30 and 60 MPa and sample thicknesses of 0.8, 1.5 and 3.0 mm are shown in Figure 1. The samples with the creep parameters 60 °C and 10 MPa, 90 °C and 10 MPa, as well as 60 °C and 30 MPa did not reach 1 % creep elongation were therefore defined as still being in the primary creep stage. For further calculations, these creep curves were extrapolated to 1 % elongation. During the secondary creep stage, defined as where elongations exceeded 1%, a nearly constant creep rate was observed, with a slight increase in creep rate as sample cross section decreased slightly, up to an elongation of 20%. Creep rate was observed to be dependent on sample thickness. For each test series, the samples with a thickness of 1.5 mm showed the highest creep rate. The samples with a thickness of 0.8 mm, with two exceptions at 10 MPa showed the lowest creep rate.

The time to achieve 1 % of the creep strain and the creep rate at 1 % creep strain were calculated by equations (1) and (2) and are shown in Table 2. The values for the test numbers 1, 2 and 4 were calculated by extrapolation to 1 %. Therefore, the values for the time to reach 1 % creep strain and the creep rate for the test numbers 1 and 2 are inaccurate.

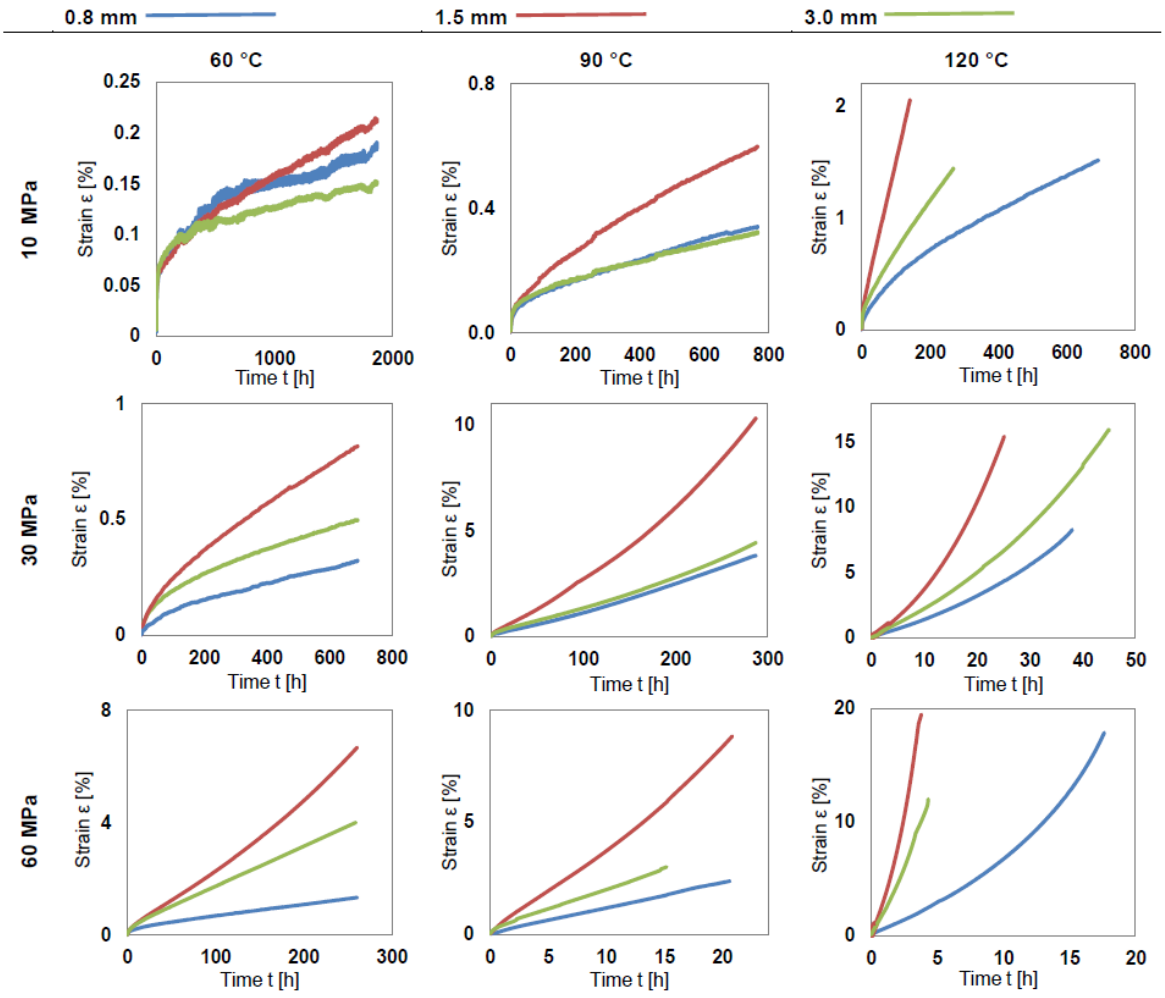


***Figure 1- Creep curves at temperatures of 60, 90 and 120 °C, stresses of 10, 30 and 90 MPa and sample thicknesses of 0.8, 1.5 and 3 mm***

*Table 2-Test results - time up to 1% creep strain (upper half); creep rate at 1% (lower half).*

| time t (hours) until 1 % creep strain | | | | | |
|---|---|---|---|---|---|
| | **no.** | **T [°C]** | **0.8 mm** | **1.5 mm** | **3.0 mm** |
| **10 MPa** | 1* | 60 | 1 665 352 | 416 237 | 64 895 698 |
| | 2* | 90 | 11 505 | 2 387 | 22 634 |
| | 3 | 120 | 360 | 70 | 194 |
| **30 MPa** | 4* | 60 | 5 694 | 1 035 | 3 223 |
| | 5 | 90 | 107 | 42 | 80 |
| | 6 | 120 | 7.8 | 3.8 | 4,5 |
| **60 MPa** | 7 | 60 | 204 | 40 | 52 |
| | 8 | 90 | 8.5 | 2.2 | 2.7 |
| | 9 | 120 | 1.14 | 0.24 | 0.27 |
| **creep rate $\dot{\varepsilon}$ (%/hour) at 1 % creep strain** | | | | | |
| | **no.** | **T [°C]** | **0.8 mm** | **1.5 mm** | **3.0 mm** |
| **10 MPa** | 1* | 60 | 0.000000079 | 0.00000041 | 0.000000002 |
| | 2* | 90 | 0.000037 | 0.000215 | 0.000016 |
| | 3 | 120 | 0.0016 | 0.0086 | 0.0027 |
| **30 MPa** | 4* | 60 | 0.000001 | 0.00001 | 0.000004 |
| | 5 | 90 | 0.0066 | 0.0163 | 0.0077 |
| | 6 | 120 | 0.1064 | 0.2209 | 0.2222 |
| **60 MPa** | 7 | 60 | 0.002 | 0.015 | 0.01 |
| | 8 | 90 | 0.10 | 0.39 | 0.33 |
| | 9 | 120 | 0.75 | 3.84 | 3.47 |

* (1, 2 and 4) In these test series the total elongation was less than 1 % and therefore the curves had to be extrapolated. All other tests have the actual measured values.

Activation energies

Table 3 shows the values of the activation energy Q, which were determined by equation (4). The value for the 3.0 mm sample at 10 MPa is very high which is due to the low creep rate of the sample at 60°C. Therefore, this value is not taken into account. The activation energy is dependent on the stress but is almost independent from the sample thickness. This means that the necessary activation energy for the creep process decreases with increasing stress. These values of activation energy are in the range of zinc-self diffusion in pure zinc [3]. The activation energy of self-diffusion of zinc along grain boundaries in pure zinc is reported as 37% less than bulk diffusion [4]. The literature values in pure zinc are lower than those in zinc alloys found in our experiments, agreeing with past work [3].

*Table 3-Summary of the calculated activation energies of the respective stresses*

| stress | sample thickness [mm] | k | Qc [kJ/mol] | Average Qc [kJ/mol] |
|---|---|---|---|---|
| **10 MPa** | 0.8 | -18 542 | 154 | 155 |
| | 1.5 | -18 751 | 156 | |
| | 3.0 | -27 553 | (229) | |
| **30 MPa** | 0.8 | -13 967 | 116 | 124 |
| | 1.5 | -14 654 | 122 | |
| | 3.0 | -15 981 | 133 | |
| **60 MPa** | 0.8 | -10 163 | 84 | 85 |
| | 1.5 | -10 370 | 86 | |
| | 3.0 | -10 140 | 84 | |

Stress exponent n

The stress exponents n were determined as shown in Figure 2. The slopes of the plotted curves give the stress exponent for each condition.

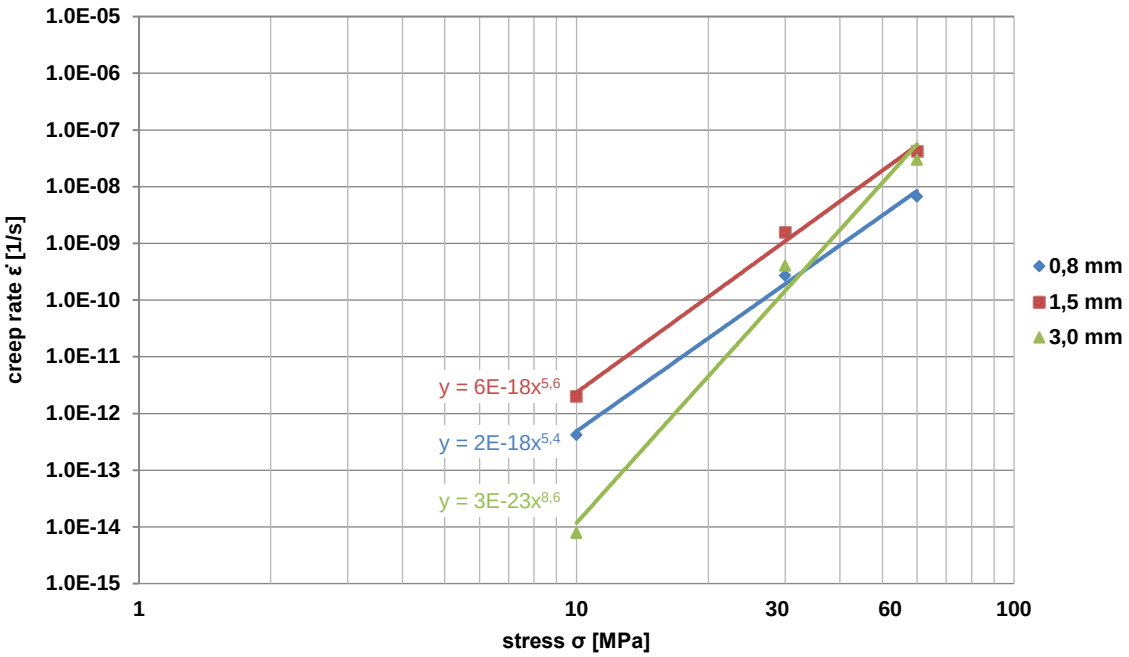


*Figure 2-Creep rate-stress curves, determination of the stress exponent*

The values of the stress exponents are listed in Table 4. The value of the 3.0 mm sample at 60 °C is very high, which is due to the very low creep rate at 10 MPa.

*Table 4-Calculated stress exponents n*

| | 60 °C | 90 °C | 120 °C |
|---|---|---|---|
| **0.8 mm** | 5.4 | 4.6 | 3.1 |
| **1.5 mm** | 5.6 | 4.2 | 3.0 |
| **3.0 mm** | 8.6 | 5.1 | 3.6 |

Creep constant

The creep constants A were calculated by equation (5) using the determined activation energies and stress exponents. The shear modulus of alloy 5 is 45 GPa. The values of the creep coefficients are listed in Table 5

***Table 5-Calculated creep constants A***

| **60 MPa** | | | |
|---|---|---|---|
| **T [°C]** | **creep constant A [1/s]** | | |
| | **0.8 mm** | **1.5 mm** | **3.0 mm** |
| **60** | $7.2 \cdot 10^{21}$ | $8.4 \cdot 10^{21}$ | $4.0 \cdot 10^{26}$ |
| **90** | $9.7 \cdot 10^{17}$ | $1.3 \cdot 10^{18}$ | $6.8 \cdot 10^{18}$ |
| **120** | $1.6 \cdot 10^{13}$ | $4.2 \cdot 10^{14}$ | $2.4 \cdot 10^{14}$ |
| **30 MPa** | | | |
| **T [°C]** | **creep constant A [1/s]** | | |
| | **0.8 mm** | **1.5 mm** | **3.0 mm** |
| **60°** | $1.6 \cdot 10^{27}$ | $5.6 \cdot 10^{27}$ | $3.6 \cdot 10^{34}$ |
| **90** | $4.5 \cdot 10^{22}$ | $1.2 \cdot 10^{23}$ | $8.9 \cdot 10^{25}$ |
| **120** | $4.9 \cdot 10^{17}$ | $1.4 \cdot 10^{19}$ | $7.0 \cdot 10^{20}$ |
| **10 MPa** | | | |
| **T [°C]** | **creep constant A [1/s]** | | |
| | **0.8 mm** | **1.5 mm** | **3.0 mm** |
| **60** | $1.4 \cdot 10^{33}$ | $6.8 \cdot 10^{32}$ | $2.7 \cdot 10^{48}$ |
| **90** | $8.6 \cdot 10^{27}$ | $1.5 \cdot 10^{28}$ | $2.0 \cdot 10^{39}$ |
| **120** | $1.8 \cdot 10^{22}$ | $4.4 \cdot 10^{23}$ | $1.4 \cdot 10^{33}$ |

## MICROSTRUCTURE

The creep behavior of the tested samples is significantly influenced by the microstructure. Goodwin et al. described five layers with different microstructures in casted Zinc alloy samples [5]. The microstructure is mainly characterized by primary η-Zn phase in a eutectic η+β' matrix. Figure 3 and Figure 4 show the microstructure in the bulk area (layer 5) and in the edge area of the 0.8 mm, 1.5 mm and 3.0 mm samples.

Each sample has a edge layer (layer 1) with a thickness of 50 µm. The edge layer has a dendritic microstructure which is becomes finer as sample thickness decreases.

The general microstructure can be described as follows, depending on the thickness of the sample:

- 0.8 mm: very fine dendritic primary η-Zn phase, lamellar or rosette shapes
- 1.5 mm: medium cellular primary η-Zn phase
- 3.0 mm: coarse cellular primary η-Zn phase

For the 1.5 mm and 3.0 mm samples, a transition from the fine dendritic layer to the cellular microstructure can be observed in moving from the edge to the bulk. The 0.8 mm sample has a dendritic structure over the entire cross-section.

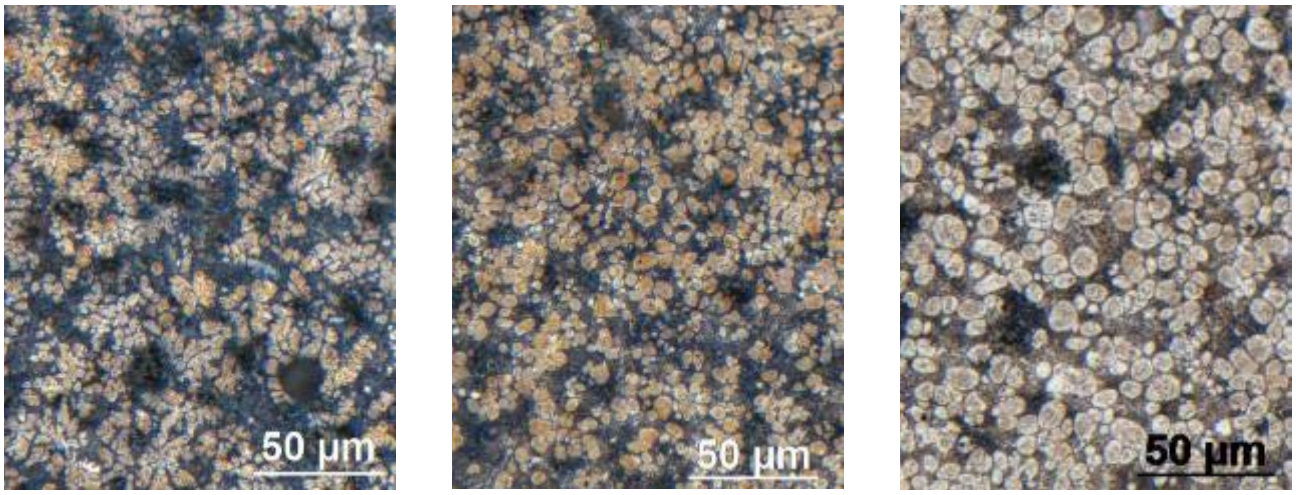


*0.8 µm* *1.5 µm* *3.0 µm*

***Figure 3- Cross section of alloy 5, aged (95°C/7d), etched in 0.5 % Nital, bulk area, 200x magnification; left: 0.8 mm sample, middle: 1.5 mm sample, right: 3.0 mm sample***

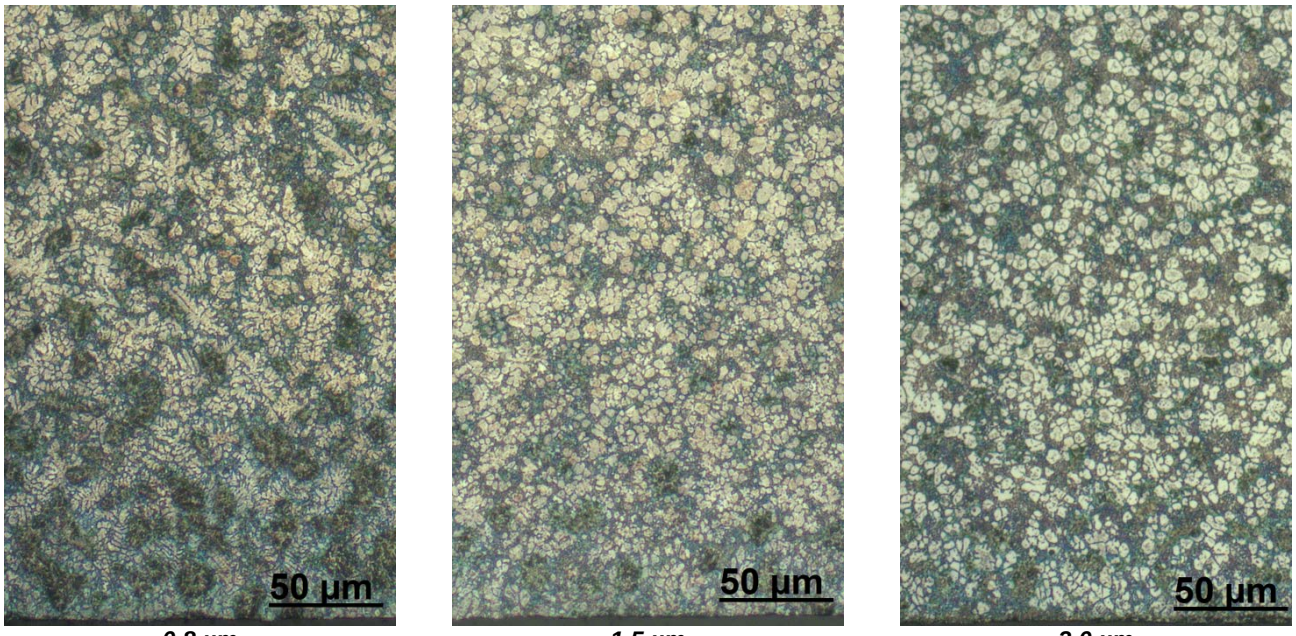


*0.8 µm* *1.5 µm* *3.0 µm*

***Figure 4-Cross section of alloy 5, aged (95°C/7d), etched in 0.5 % Nital, edge area, 200x magnification; left: 0.8 mm sample, middle: 1.5 mm sample, right: 3.0 mm sample***

To compare the microstructure of each sample thickness, the volume fraction of the primary η-Zn phase and the average phase diameter were determined by quantitative microstructure analysis. A grid was placed over the micrograph and the number of crossings in the primary phase was determined. The volume fraction of the primary η-Zn phase was calculated as the proportion of the number of crossings in the primary phase and the total number of crossings. To determine the average phase diameter a straight line with 200 µm length was laid over the micrograph and the number of crossed dendrites was determined. The average phase diameter d was calculated with the following formula, using the volume fraction of the η-Zn phase $V_V$, the length of the straight line $l$ and the number of crossed dendrites $n$:

$$d = \frac{V_V \cdot l}{n}$$

In Table 6 the values are given for each layer with an indication of the range of each layer. The average phase diameter of the 0.8 mm sample in layers 1-3 could not be determined due to the fine lamellar shape of the dendrites.

*Table 6-Volume fraction of η-Zn and average phase diameter for each layer*

| Volume fraction η-Zn $V_V$ / average phase diameter d | | | | | | |
|---|---|---|---|---|---|---|
| | | **Layer 1** | **Layer 2** | **Layer 3** | **Layer 4** | **Layer 5** |
| **0.8 mm** | **range [µm]** | 0-40 | 40-100 | 100-200 | 200-300 | 300-400 |
| | **$V_V$ [%]** | 83 | 84 | 66 | 69 | 69 |
| | **d [µm]** | | | | 3.4 | 3.5 |
| **1.5 mm** | **range [µm]** | 0-50 | 50-125 | 125-200 | 200-400 | 400-750 |
| | **$V_V$ [%]** | 83 | 74 | 73 | 64 | 66 |
| | **d [µm]** | 3.8 | 4.3 | 4.4 | 4.6 | 5.7 |
| **3.0 mm** | **range [µm]** | 0-50 | 50-150 | 150-300 | 300-500 | 500-1500 |
| | **$V_V$ [%]** | 72 | 65 | 65 | 59 | 80 |
| | **d [µm]** | 3.7 | 4.2 | 5.6 | 7.3 | 7.6 |

## THE INFLUENCE OF THE DENDRITIC STRUCTURE ON THE CREEP RATE

To verify the influence of the dendritic microstructure on the creep behavior, 4 additional creep tests were performed. The creep test parameters were set to 120°C / 30 MPa. For the first three samples, the layers 1-4 were removed to examine the creep properties of the bulk area. The fourth sample, from which no metal was removed, was subjected to a heat treatment with the aim to transform the fine dendritic structure into a spherical structure. A brief overview of the test variables is given below:

1. Grinding by hand – reduce casting thickness from 1.5 mm to 0.8 mm

A sample with 1.5 mm thickness was grinded on a belt grinding machine. 0.35 mm were removed from each side to reach the target thickness of 0.8 mm.

2. Milled – 1.5 mm to 0.8 mm

Same procedure as 1. but the sample was milled to guarantee a uniform sample thickness of 0.8 mm.

3. Milled – 3.0 mm to 0.8 mm

A sample with 3.0 mm thickness was milled to a final dimension of 0.8 mm, removing equal metal from each side.

4. Heat treatment + aged – 0.8 mm

The annealing temperature was 325°C for 24 hours. Then the samples were quenched in water (at RT) in order to freeze the resulting microstructure. As the ageing processes were also neutralized by the heat treatment, subsequent ageing at 95°C for 7 days was performed. Figure 5 shows a comparison of the dendritic structure before (left) and after (right) the heat treatment.

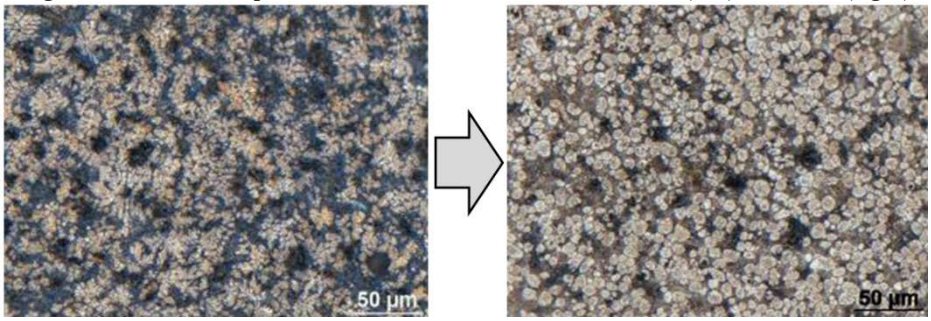


***Figure 5-Cross section of a 0.8 mm sample before and after the heat treatment***

### Additional Creep tests

The results of the additional creep tests are shown in Figure 6. The creep curves of the first series (0.8 mm, 1.5 mm, 3.0 mm) with the same parameters are added to the diagram for a direct comparison.

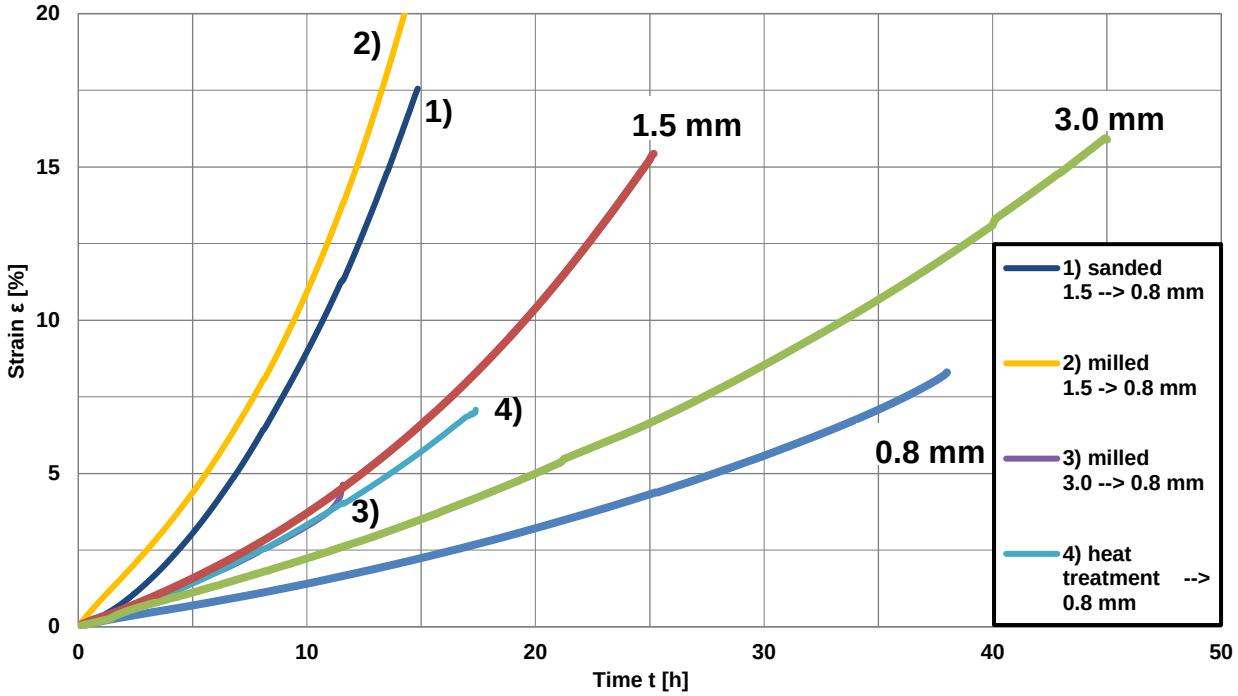


***Figure 6-Additional test series 10 under different conditions (120 ° C / 30 MPa)***

The creep rates of samples 1 and 2 are significantly higher than the original 1.5 mm sample. By removing the layers 1-4 by grinding or milling the creep resistance of the samples was decreased. Sample 3 with removed layers 1-4 shows a higher creep rate and so a decreased creep resistance compared to the 3 mm sample. The heat-treated sample 4 also shows a significant increase in the creep rate. It can be expected that the fine lamellar dendrites of the 0.8 mm sample were successfully converted into coarse cellular dendrites. Since the creep curve of the heat-treated sample is directly above the curve of sample 3, the microstructure of both samples seems to be similar. Sample 3 consists of layer 5 of the 3 mm sample.

## DISCUSSION

It is well-established that the mechanism of creep in zinc die castings is diffusional flow; this is again confirmed by the results of Table 3 that show values of activation energy agreeing with the activation energy of zinc self-diffusion, and that this value is independent of section thickness. It is usually observed that creep rate decreases with increasing grain size, and this trend is seen when comparing the 1.5 mm with the 3.0 mm casting thickness results. As explained by Nabarro and de Villiers [6], larger grains suppress the faster grain boundary diffusional flow more than the slower diffusional flow of vacancies and counterpart interstitials through the lattice of the bulk grain. On the Ashby map of creep mechanisms in Figure 7, this means that larger-grained samples shift more into the domain of lattice diffusional flow (Nabarro-Herring creep), and further away from the grain boundary flow domain (Coble creep).

For the 0.8 mm samples, the situation is different. While the shape of the dendrites of the 1.5 mm and 3.0 mm samples is largely spherical, the dendrites of the 0.8 mm samples are finely dispersed in the eutectic matrix as lamellas or rosettes. This microstructure has the highest creep resistance and was also found in the layers 1 and 2 of the 1.5 mm and 3.0 mm samples. By removing the edge area of the samples, the creep resistance decreased significantly. As the creep tests with the heat-treated sample 4 show, the fine dendritic microstructure can be converted to a coarse spherical microstructure, which has a lower creep resistance.

For the 0.8 mm samples, there is a much larger fraction of eutectic than in the 1.5 mm and 3.0 mm thick samples. As with all castings of this alloy composition, the eutectic is a fine-scale mixture of Zn-rich and Al-rich phases. At the high solidification rate experienced in the 0.8 mm thick samples, the eutectic phases are mixed on a submicron scale. Although the eutectic interphase orientation mismatch has not been studied in zinc diecasting alloys, it has been reported for the Mg-Al eutectic that this mismatch decreases with increasing growth rate [7]. In the Nabarro-Herring creep mechanism, imposition of an axial stress results in creation of vacancy-interstitial atom pairs on grain boundaries normal to the tensile axis. The vacancies diffuse into the bulk of the crystal; the interstitials remain behind and form additional atom layers on the grain boundaries normal to the

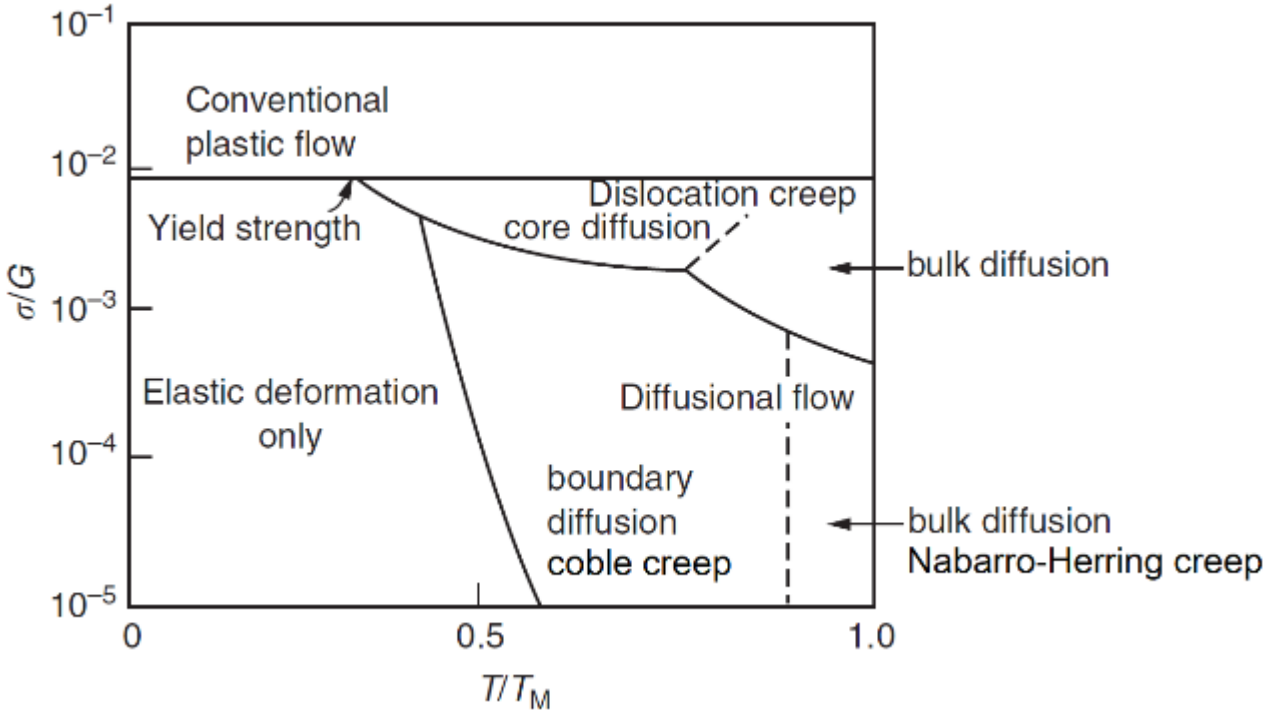


***Figure 7-Deformation mechanisms at different stresses and temperatures [8].***

tensile axis, resulting in axial elongation. The excess vacancies then diffuse to grain boundaries parallel to the tensile axis, resulting in transverse thinning of the sample. A significantly larger amount of interdendritic eutectic with a much smaller overall inter-lattice mismatch than present in the more slowly cooled samples, not only between the eutectic constituents but also between the eutectic and primary phase, would therefore reduce the grain boundary energies in this eutectic and therefore the driving force for both formation of new vacancies and interstitials together with the migration of vacancies to grain boundaries. This is supported by the results of the 0.8 mm samples that were heat treated at 325 °C for 24 h; the decrease in fraction eutectic and increase in primary phase size permit the heat-treated sample to behave more like the thicker test samples.

## REFERENCES


1. F. C. Porter, Zinc Handbook: Properties, Processing, and Use in Design, Marcel Dekker, New York, NY, 1991 ISBN 0-8247-8340-9
2. W. Leis, “Comparison of all die cast zinc alloys with regard to their creep behavior taking into account aging”, Gießerei Kolloquium 2016, May 11-12, 2016, University of Aalen, Germany
3. J.E. Hilliard, B.L. Averbach, M. Cohen, Self- and Inter-diffusion in Aluminum-Zinc Alloys”, Acta. Met., 7 (2) February 1959, 86-92
4. E.S. Wajda, “Grain Boundary Self-Diffusion in Zinc” Acta Met 2 (2) March 1954, 184-187
5. F. Goodwin et al., "The Influence of Casting Process Parameters on the Properties and Microstructures of Zinc Alloys 3 and 5," Proceedings of the 16th International NADCA Die Casting Congress and Exposition, September 30-October 3, 1991, Detroit, MI.
6. F.R.N. Nabarro and H.L. de Villiers, “The Physics of Creep”, 1995, Taylor & Francis, ISBN 085066 852 2
7. S. Guldberg and N. Ryum, “Microstructure and crystallographic orientation relationship in directionally solidified Mg–Mg17Al12-eutectic”, Materials Science and Engineering A 289(1):143-150, August 2000, DOI: 10.1016/S0921 5093(00)00945-X
8. M. F. Ashby and D. R. H. Jones, “Engineering Materials 1” Oxford, Elsevier, 2005. ISBN 0-08-026138-8